*Int. J. Electrochem. Sci.*, 6 **(2011)** 2162 - 2170

International Journal of
ELECTROCHEMICAL
SCIENCE
www.electrochemsci.org

# Synthesis, Characterization of $In_2O_3$ Nanocrystals and Their Photoluminescence Property

*Guodong Liu*[*]

Department of Chemistry and Chemical Engineering, Jining University, Jining 273155 P. R. China
[*]E-mail: liugd2011@hotmail.com

*Received:* 25 April 2011 / *Accepted:* 15 May 2011 / *Published:* 1 June 2011

$In_2O_3$ nanocrystals have been solvothermally synthesized using indium acetylacetonate as precursor. The morphologies of nanocrystals, e.g. nanocuboids and nanoflowers, could be tunable by adjusting the solvent such as ethanol, toluene. The as-prepared products were characterized by X-ray powder diffraction (XRD), transmission electron microscope (TEM), High-Resolution transmission electron microscope (HR-TEM) and Fourier transform infrared (FT-IR) techniques in detail. UV-vis absorption spectroscopy and photoluminescence spectrums of nanocrystals are also detected.

**Keywords:** $In_2O_3$ Nanocuboids, Self-assemble, Photoluminescence

## 1. INTRODUCTION

As an important transparent conducting metal oxides (TCOs) with a wide band-gap of 3.55-3.75 eV, indium oxide ($In_2O_3$) has attracted considerable attention because of its high electron affinity and low electron effective mass and increasingly extensive applications in fuel cells [1-4], sensors [5], nanoscale transistors [6], and flat-panel display materials [7], etc. In the past decade, $In_2O_3$ nanocrystals with different morphologies such as nanoparticles [8-10], nanowires [11], nanorods [12], nanoribbons/nanobelts [13,14], nanocrystal chains [15], nanotubes [16,17], nanotowers [18], hollow spheres [19,20], microarrows [21] have been successfully prepared. Of course, a lot of synthesis methods have been developed.

More recently, there has been considerable attention on the synthesis of $In_2O_3$ nanostructures with well-defined nanocuboids in order to endow nanomaterials with additional properties or potiential applications [22]. Based on so many literature Shi and Xu synthesized the nanocuboids by chemical vapor phase deposition (CVD) [23], but hydrothermal [8,24] or aqueous solvothermal methods [25] are

still the mostly used. However, it is very difficult to obtain the $In_2O_3$ nanocuboids directly using solution synthesis method, in which the calcination of corresponding hydrothermal precursors, such as $In(OH)_3$ and InOOH is necessary. Of course, there are some exceptions. Yang prepared the $In_2O_3$ nanocuboids used a one-step aqueous solvothermal process [25]. Among the above methods, it can be concluded that $H_2O$ plays a crucial role and hydrolyzation of $In^{3+}$ is absolutely necessary. Hence, how to prepare highly crystalline $In_2O_3$ nanocuboics using a more convenient direct synthesis route is urgent. So far, the synthesis of $In_2O_3$ nanocuboids in nonaqueous system is rarely reported. In the present work, $In_2O_3$ nanocuboids were synthesized via one-step ethanol solvothermal treatment using indium acetylacetonate as precursor in a simple surfactant-free nonaqueous system. The nanocuboids with controlled size are well-faceted and all of their corners and edges can be clearly distinguished. It is worth noting that the size of nanocuboids here is less than the previous reports obviously. Furthermore, the morphologies of nanocrystals could be tunable by adjusting the solven, and a possible growth mechanism was also proposed.

## 2. EXPERIMENTAL SECTION

### *2.1. Synthesis.*

In a typical synthesis, 0.5 g (1.21 mmol) of $In(acac)_3$ was added to 25.0 mL solvent (ethanol, *n*-buthanol, *n*-octanol or toluene).

The mixture was transferred into Teflon-lined autoclaves which was heated to at 200 °C and kept for 48 h. The product was collected by centrifugization, washed with ethanol for several times and dried at 60 °C for 2 h in air.

### *2.2. Characterization.*

X-ray diffraction (XRD) patterns of the samples were recorded on an X-ray diffractometer (Rigaku D/Max 2200PC) with a graphite monochromator and CuKα radiation (λ=0.15148 nm) in the range of 10-80° at room temperature while the voltage and electric current were held at 40 kV and 20 mA.

The morphology and microstructure of the products were determined by transmission electron microscopy (TEM, JEM-100CXII) with an accelerating voltage of 80 kV and high-resolution TEM (HR-TEM, GEOL-2010) with an accelerating voltage of 200 kV. Thermal gravimetric (TG) analysis was conducted on a thermal analyzer (TGA/SDTA, $851^e$ METTLER) with the heating rate of 10.0 $°C \cdot min^{-1}$ under an air flow of 20.0 $mL \cdot min^{-1}$. The Fourier transform infrared (FT-IR) spectra were recorded on a Nicolet 5DX-FTIR spectrometer using the KBr pellet method in the range of 400-4000 $cm^{-1}$.

Atomic force microscopy (AFM) images were taken with a Nanoscope IIIa Multimode AFM (Digital Instruments Inc.) at room temperature. Tapping mode was utilized at a scan rate of 1.0 Hz with a silicon cantilever having resonance frequency about 200 kHz.

## 3. RESULTS AND DISCUSSION

The $In_2O_3$（indium oxide） nanocrystals obtained in different solvents including ethanol and toluene exhibited same morphology but different size, which is denoted as S1 (from ethanol), S2 (from toluene) respectively. All the XRD patterns of the samples exhibit the same reflections, indicating the same phase structure of the samples derived from different solvents.

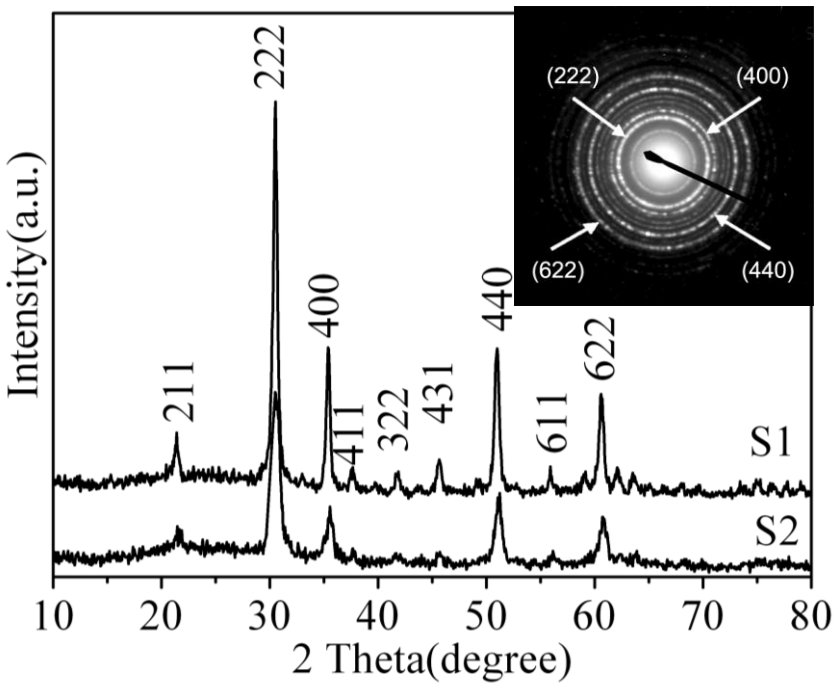


**Figure 1.** XRD patterns of the as-prepared $In_2O_3$ from different solvents. The inserted is electron diffraction pattern of $In_2O_3$ nanocuboids obtained in ethanol

(See Fig. 1) All the XRD reflections can be indexed to the cubic $In_2O_3$ (JCPDS, No. 65-3170), no other peaks can be observed, revealing their phase-pure cubic structures. The electron diffraction pattern (SAED) of $In_2O_3$ nanocuboids obtained in ethanol is also consistent with cubic $In_2O_3$ with strong ring patterns due to (222), (400), (440), and (622) planes (Inserted Fig. 1). The sizes of the products obtained from ethanol and toluene are21.8, 6.0 nm respectively. Further calculation revealed that the cell parameters of the samples are respectively 1.0138 and 1.0142 nm, which are in well agreement with the reported data of a=1.0140 nm (JCPDS, No. 65-3170). The data was collected using KCl as standard graph and the scan speed was one degree per minute.

TEM images (Fig. 2) of the samples obtained from ethanol show that the nanocuboids are with smooth and regular quadrangle surface. When the solvent changed from ethanol to toluene, the longest side length of the nanocuboids decreased from ca.20.0 nm to 5.0 nm, and the shortest side decreased from ca.8.0 nm to ca.3.0 nm respectively. (Fig. 2)The HR-TEM image of a single nanocuboid shows the clear resolved lattice fringes in the visible range, indicating its single crystalline nature. The lattice distances 0.293 nm and 0.253 nm can be readily indexed to {222} and {400} planes of cubic $In_2O_3$,

indicating that all the nanocuboids from different solvents exhibited the same preferential crystal plane of {110}.

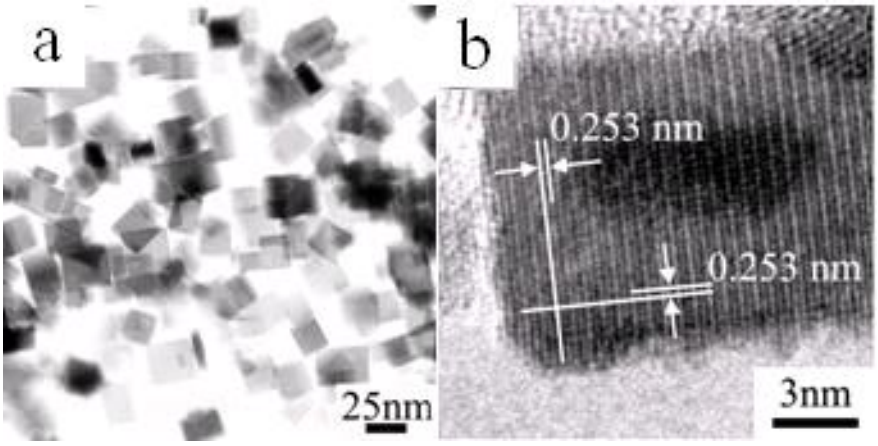


**Figure 2.** TEM ,HR-TEM images of the as-prepared $In_2O_3$ nanocubics (S1).

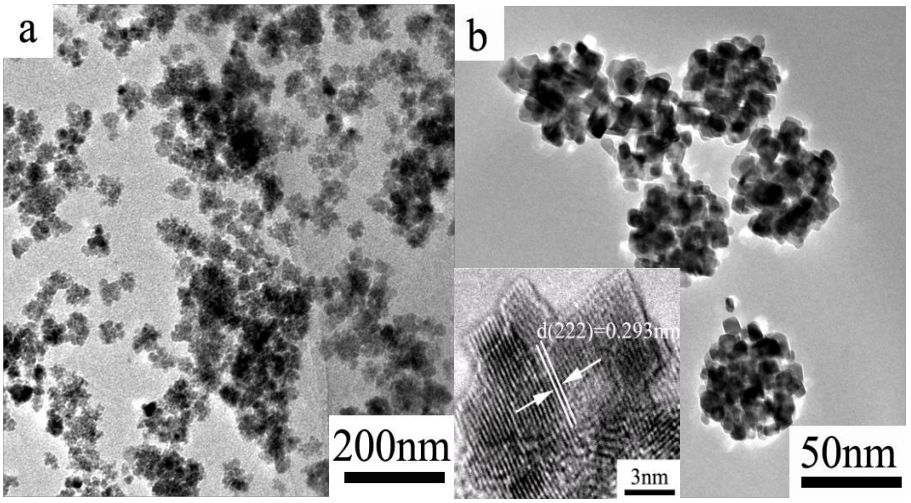


**Figure 3.** TEM images of the as-prepared $In_2O_3$ nanocubics (S2)(a,b). The inserted is HR-TEM images.

In order to clarify the simple thermal decomposition of the precursor in the reaction process, XRD and IR techniques were used to track the solvothermal process in ethanol (See Fig. 4). XRD patterns of the samples obtained at different solvothermal reaction times shows that there is no intermediate during the formation of $In_2O_3$ nanocuboics. The corresponding IR spectra revealed that the absorption of acetylacetonate species decreased gradually during the solvothermal process and completely disappeared after solvothermal treated for 36 h. From the TEM images, it can be seen that the size of nanocrysals increased slightly after crystallized (See Fig. 5). So, the size of nanocuboids was mainly determined by the process of thermal decomposition of the precursor. The thermal stability of the precursors is strongly dependent on the dielectric constants of the solvents. The dissociation of ionic bonds and the weakening of electrostatic interactions within crystals are easier in a higher

dielectric constant medium [26]. During the solvothermal process under 200 ℃, the $In_2O_3$ nanocrystals can be obtained less than 4 h in ethanol (See Fig. 4A).

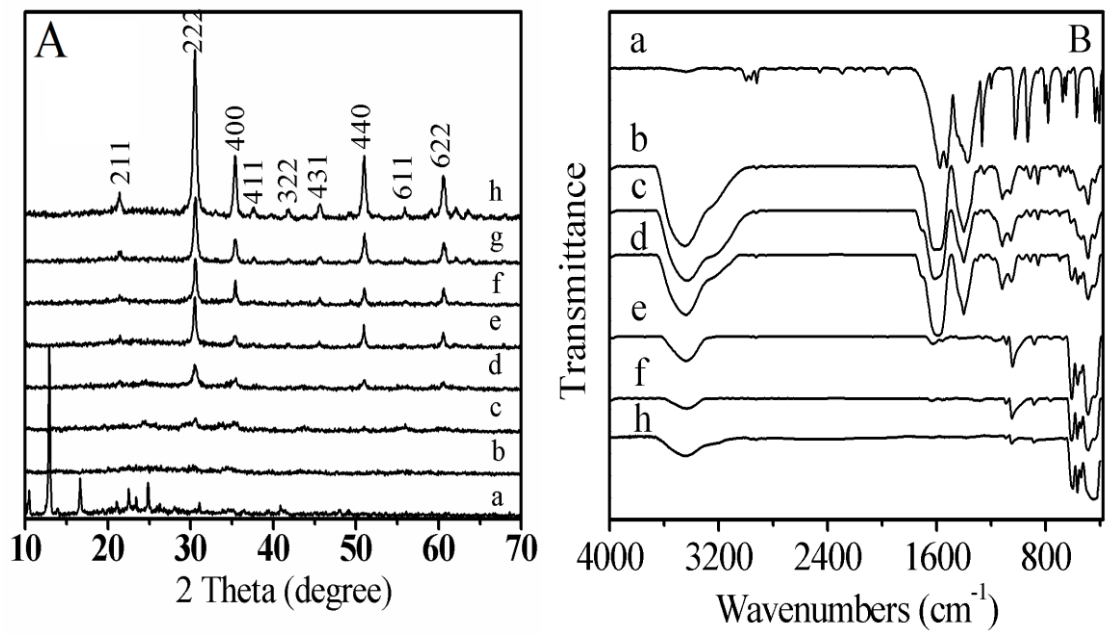


**Figure 4.** XRD patterns (A) and IR spectra (B) of the samples obtained at different reaction times. (a) 0 h, (b) 4 h, (c) 8 h, (d) 12 h, (e) 24 h, (f) 36 h, (g) 48 h.

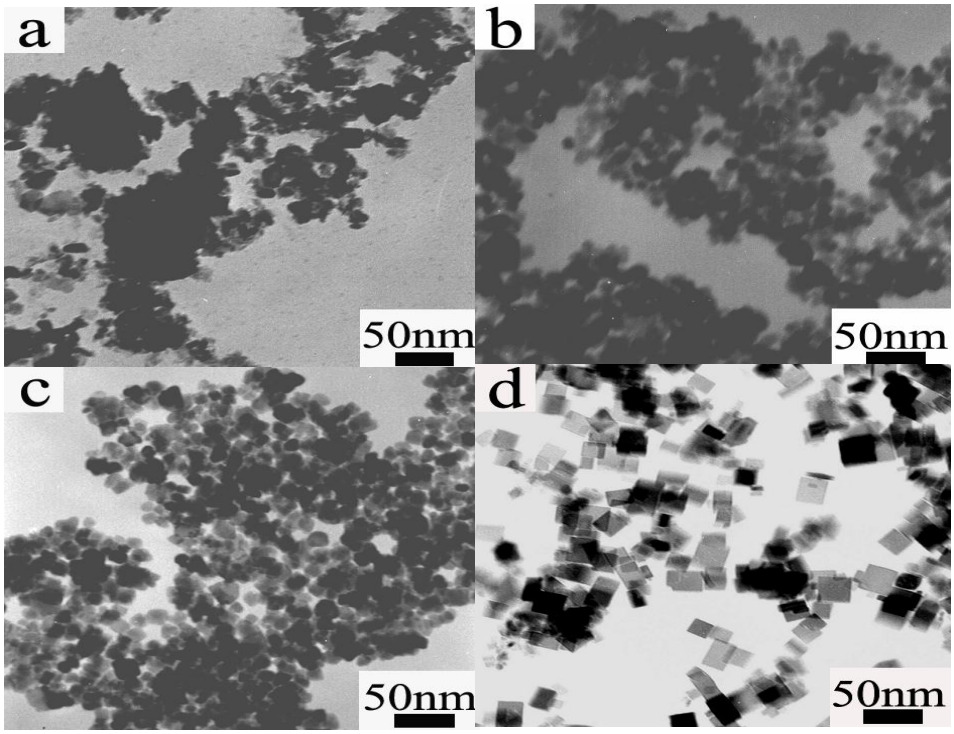


**Figure 5.** TEM images of the products obtained at different time in ethanol (a) 4h, (b) 12h, (c) 24h, (d) 48h.

However, the same products obtained in toluene need more than 8 h (See Fig. 6). As the decomposition of $In(acac)_3$was very slow in toluene, the growth speed of $In_2O_3$ nanocrystals was also slow. In this case, the speed of collision between the small nanocrystals is larger than the growth rate of nanocrystals in toluene system. In order to decrease the surface energy, the preformed $In_2O_3$ nanocrystals tend to aggregate randomly instead of growing larger. When the reaction time was increased to 48 h, 3-dimensional (3D) hierarchical flowerlike nanostructure of $In_2O_3$ composed of nanocuboids of ca. 3-5 nm size, can be obtained (See Fig. 3). Thus it is concluded that controlled the size of the nanocrystal could be readily realized by simply adjusting the reaction medium.

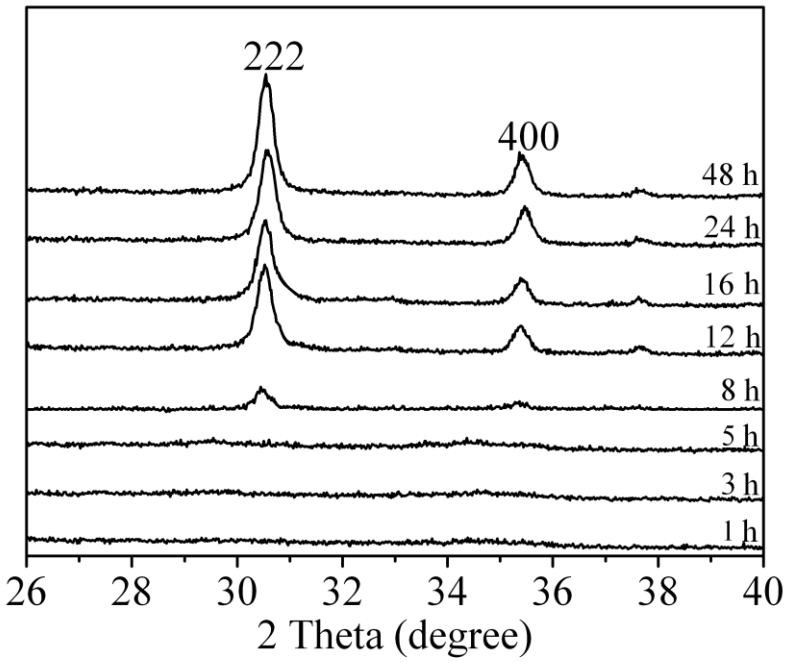


**Figure 6.** XRD patterns of the samples obtained via toluene solvothermal process at different reaction times.

The IR spectra of the samples from ethanol and toluene are almost the same, indicating that their surface states are similar. (See Fig. 7a) The bands around 3400 $cm^{-1}$ and 1630 $cm^{-1}$ are attributed to the absorptions of hydroxyls from absorbed water or alcohols, and those at 2925 $cm^{-1}$, 2858 $cm^{-1}$ and 1416 $cm^{-1}$ can be ascribed to the C-H vibrations of the organics. The band at 1050 $cm^{-1}$ is attributed to the absorption of C-O vibration, while the absorptions around 500 $cm^{-1}$ are due to the In-O vibrations [16]. As an exception, a weak absorption at 1568 $cm^{-1}$ appeared on the IR spectrum of the nanocrystals from toluene, which should be attributed to the C=O vibrations from the acetylacetone species [27]. The result indicates that the surface species of the $In_2O_3$ nanocrystals from different solvents are mainly the alcohol molecules, and a few of acetylacetone species also exist on the surface of the $In_2O_3$ nanocrystals from toluene. Based on the experiments, the acetylacetone species coordinated to $In^{3+}$ cations on the particle surface could be substituted by the alcohol molecules during

the solvothermal process, while toluene could not coordinated to $In^{3+}$ and only part of the acetylacetone species were replaced by the alcohol molecules when the nanocrystals were washed by ethanol.

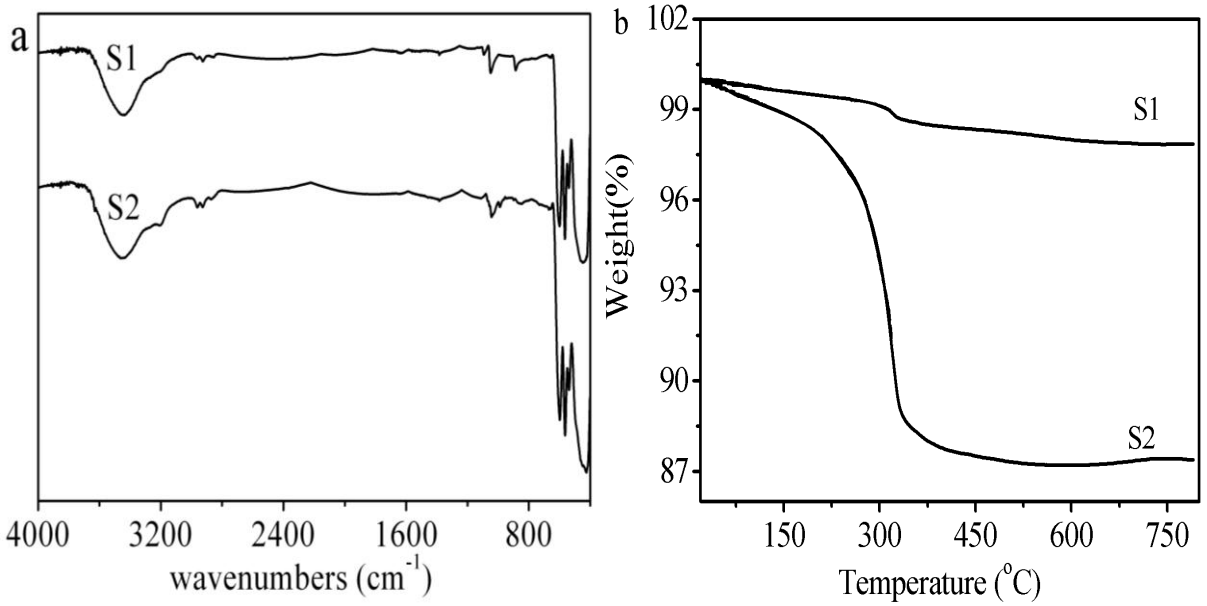


**Figure 7.** IR spectra (a) and TG curves (b) of the samples from different solvents.

The corresponding TG curves show three steps of weight loss in the similar temperature range. (See Fig. 7b)The first one occurred from room temperature to 240 °C, which increased from 0.1% to 2.6% respectively with the particle size decreasing from S1 to S2. The second one centered at 300 °C changed from ca.1.5% and 9.5%. With the temperature increased higher than 340 °C, all the samples only show a small amount of weight loss about less than 1.0%. Combined with the IR analyses, it is concluded that the first weight-loss might be due to the removal of the surface absorbed alcohol and water molecules, and the second one resulted from the decomposition of the alcohol molecules. A few acetylacetone species combined with the $In^{3+}$ cations led to an obvious exothermic effect on the corresponding DSC curves. The last one should be attributed to the removal of the hydroxyls on the particle surface. The increase in weight-loss is resulted from the increasing of the surface area with the size decreasing. Based on the IR and TG analyses, it could be concluded that the $In_2O_3$ nanocrystals with different sizes showed similar surface species only with different amount, which favors the investigation of the effect of the particle size on the physical properties.

The Uv-vis absorption spectra of nanocuboids with different sizes show absorption maxima at 300-310 nm (Fig. 4a).Compared to the absorption at 330 nm (3.75 eV) of bulk $In_2O_3$ [10], a blue-shift is observed due to the weak quantum confinement effect [9]. The PL (all the samples excited at 330 nm, room temperature) emission of the $In_2O_3$ nanocrystals with different sizes (Fig. 7b) are nearly identical with strong PL peaks centered at 451 nm (blue), 548 nm, 568 nm (yellow), and 616 nm (orange). Cubic $In_2O_3$, as a typical n-type semiconductor, has an oxygen-deficient fluorite structure with twice the unit-cell edge of the corresponding fluorite cell and with 1/4 of the anions missing in an

ordered way, which would induce the formation of new energy levels in the band gap [28]. Furthermore, $In_2O_3$ nanocuboids with a high aspect ratio and peculiar morphologies should also favor the existence of large quantities of oxygen vacancies and their visible emission from oxygen deficiencies is easily detectable. Finally, the PL spectrum of $In_2O_3$ nanocrystals seems to be independent of the particle size but the synthesis route.

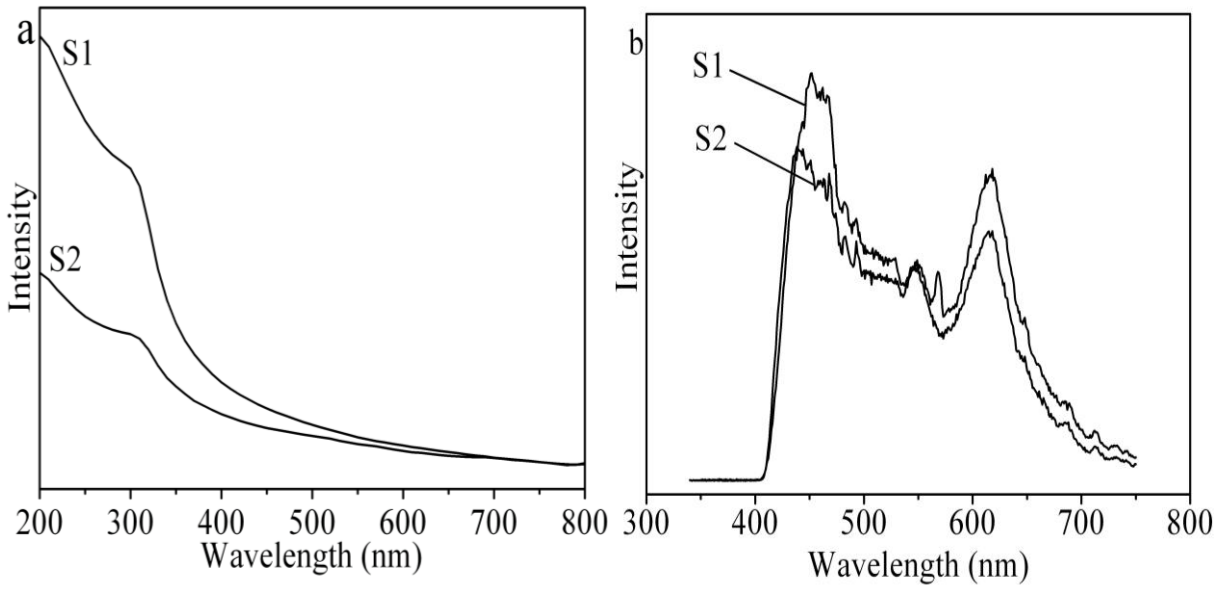


**Figure 8.** UV-vis spectra (a) and PL spectra (b)of $In_2O_3$ nanocuboids from different solvents.

## 4. CONCLUSIONS

$In_2O_3$ nanocuboids were synthesized via a simple solvothermal process using indium acetylacetonate as precursor. The sizes of nanocuboids can be tuned from 20 nm to 6 nm by simply adjusting the solvents. The formation of the $In_2O_3$ nanocuboids is due to the solvothermal decomposition of the indium acetylacetonate, and the different dielectric constants of the solvents resulted in the different particle sizes in different solvents . The UV absorption of $In_2O_3$ nanocrystals occurs at 300-310 nm, indicating the existence of a weak quantum confinement effect. The PL emissions of as-prepared $In_2O_3$ nanocuboids centered at 451 nm, 548 nm, 568 nm, and 616 nm were originated from various oxygen vacancies. The as-obtained $In_2O_3$ nanocubics might perform better in optical and electric devices, solar cells, liquid crystal devices and detectors because of novel shape of their building blocks and controllable thickness.

ACKNOWLEDGEMENTS.
This work is supported by Doctoral Foundation of Shandong Province (BS2010CL009) the Research Foundation of Jining University (No.2010KJLX03) and Pre-research Fund of National Foundation (2011YYJJ01).

**References**


1. J. Parrondo, R. Santhanam, F. Mijangos, B. Rambabu, *Int. J. Electrochem. Sci*., 5 (2010) 1342-1354.
2. A. O. Neto, R. W. R. Verjulio-Silva, M. Linardi, E.V. Spinace, *Int. J. Electrochem. Sci*.4 (2009) 954– 961.
3. J. Arun kumar, P. Kalyani, R. Saravanan, *Int. J. Electrochem. Sci.* 3 (2008) 961 – 969.
4. B. Krishnamurthy, S. Deepalochani, *Int. J. Electrochem. Sci*., 4 (2009) 386 – 395.
5. D.Zhang, Z. Liu, C.Li, T. Tang, X.Liu, S.Han, B.Lei, C.Zhou, *Nano Lett*. 4(2004) 1919-1923.
6. P. Nguyen, H. T.Ng, T.Yamada, M. K.Smith, J.Li, J.Han, M.Meyyappan, *Nano Lett*. 4(2004)651-657.
7. J.Cui, A.Wang, N. L.Edleman, J.Ni, P.Lee, N. R.Armstrong, T. J.Marks, *Adv. Mater.* 13(2001)1476-1480.
8. Q.Tang, W. Zhou, W.Zhang, S.Qu, K.Jiang, W.Yu, Y.Qian, *Cryst. Growth & Des*. 5(2005) 147-156.
9. C.Lee, M.Kim, T.Kim. A.Kim, J.Paek, J.Lee, Choi, S.; Kim, K.; Park, J.; Lee, K. J. *Am. Chem. Soc*. 128 (2006)9326-9327.
10. Q.Liu, W.Lu, A. Ma, J.Tang, J.Lin, J. Y.Fang, *J. Am. Chem. Soc.* 127(2005)5276-5277.
11. C.Liang, G.Meng, Y.Lei, F. Phillipp, L. Zhang, *Adv. Mater*. 13(2001) 1330-1333.
12. J.Yang, C.Lin, Z.Wang, J.Li, *Inorg. Chem*. 45(2006)8973-8979.
13. J.Jeong, J.Lee, C. Lee, S.An, G. Yi, *Chem. Phys. Lett*. 384(2004)246-250.
14. Z.Pan, Z.Dai, Z. Wang, *Science* 291(2001) 1947-1949.
15. J.Lao, J.Huang, D.Wang, Z.Ren, *Adv. Mater*. 16 (2004)65-69.
16. C.Chen, D.Chen, X.Jiao, C.Wang, *Chem. Commun*. (2006) 4632.
17. Y.Li, Y.Bando, D. Golberg, *Adv. Mater*. 15(2003)581-585.
18. Y.Yan, Y.Zhang, H.Zeng, L.Zhang *Cryst. Growth & Des.* 7 (2007) 940-943.
19. P. Zhao, T.Huang, K.Huang, *J. Phys. Chem*. C 111(2007) 12890-12897.
20. B. Li, Y.Xie, M.Jing, G. Rong, Y.Tang, G. Zhang, *Langmuir* 22(2006)9380-9385.
21. D. A.Magdas, A.Cremades, J. Piquerasb, *Appl. Phys. Lett*. 88(2006) 113107-2.
22. H.Zhu, X.Wang, F.Yang, X.Yang, *Cryst. Growth & Des*. 8(2008) 950-956.
23. M.Shi, F.Xu, *J. Phys. Chem*. C 111(2007)16267-16271.
24. Z.Zhuang, Q.Peng, J.Liu, X.Wang, Y.Li, *Inorg. Chem*. 46(2007)5179-5187.
25. J.Yang, C. Li, Z.Quan, D.Kong, X.Zhang, P.Yang, J. Lin, *Cryst. Growth & Des*. 8(2008) 695-699.
26. G.Garnweitner, J.Hentschel, M.Antonietti, M. Niederberger *Chem. Mater*. 17(2005) 4594-4599.
27. D.Chu, Y.Zeng, D.Jiang, J. Xu, *Nanotechnology* 18(2007)435605-436510
28. H.Cao, X.Qiu, Y.Liang, Q. Zhu *Appl. Phys. Lett.* 83(2003) 761-763.